OATAO

Open Archive Toulouse Archive Ouverte

Open Archive Toulouse Archive Ouverte (OATAO)

OATAO is an open access repository that collects the work of Toulouse researchers and makes it freely available over the web where possible

This is an author's version published in: **http://oatao.univ-toulouse.fr/27607**

Official URL: https://doi.org/10.1158/2326-6066.CIR-19-0855

Any correspondence concerning this service should be sent to the repository administrator: tech-oatao@listes-diff.inp-toulouse.fr

Dual Relief of T-lymphocyte Proliferation and Effector Function Underlies Response to PD-1 Blockade in Epithelial Malignancies

Camille Charlotte Balança[1], Clara Maria Scarlata[1], Marie Michelas[1], Christel Devaud[1], Victor Sarradin[1,2], Camille Franchet[3,4], Carlos Martinez Gomez[1,5], Carlos Gomez Roca[1,2], Marie Tosolini[6], Diana Heaugwane[7], Françoise Lauzéral Vizcaino[1,4], Lucile Mir Mesnier[8], Virginie Féliu[1], Carine Valle[6], Frédéric Pont[6], Gwénaël Ferron[5], Laurence Gladieff[2], Stéphanie Motton[9], Yann Tanguy Le Gac[9], Agnès Dupret Bories[5], Jérôme Sarini[5], Benjamin Vairel[9], Claire Illac[7], Aurore Siegfried Vergnon[3], Eliane Mery[7], Jean Jacques Fournié[1], Sébastien Vergez[4,9], Jean Pierre Delord[1,2,4], Philippe Rochaix[7], Alejandra Martinez[1,5], and Maha Ayyoub[1,4,8]

Although understanding of T cell exhaustion is widely based on mouse models, its analysis in patients with cancer could provide clues indicating tumor sensitivity to immune checkpoint blockade (ICB). Data suggest a role for costimulatory pathways, particularly CD28, in exhausted T cell responsiveness to PD 1/PD L1 blockade. Here, we used single cell transcriptomic, phenotypic, and function al approaches to dissect the relation between CD8^{+} T cell exhaus tion, CD28 costimulation, and tumor specificity in head and neck, cervical, and ovarian cancers. We found that memory tumor specific CD8^{+} T cells, but not bystander cells, sequentially express immune checkpoints once they infiltrate tumors, leading, *in situ*, to a functionally exhausted population. Exhausted T cells were none theless endowed with effector and tumor residency potential but exhibited loss of the costimulatory receptor CD28 in comparison with their circulating memory counterparts. Accordingly, PD 1 inhibition improved proliferation of circulating tumor specific CD8^{+} T cells and reversed functional exhaustion of specific T cells at tumor sites. In agreement with their tumor specificity, high infiltration of tumors by exhausted cells was predictive of response to therapy and survival in ICB treated patients with head and neck cancer. Our results showed that PD 1 blockade mediated proliferation/reinvigoration of circulating memory T cells and local reversion of exhaustion occur concurrently to control tumors.

Introduction

CD8^{+} T cells targeting cancer antigens infiltrate tumors, and the extent of the CD8^{+} T cell infiltrate correlates with better prognosis (1). Nonetheless, expression of inhibitory immune checkpoints (IC), such as PD 1, CTLA 4, TIGIT, and TIM 3, in tumor infiltrating CD8^{+}

T cells contributes to their functional exhaustion (2, 3). Therapeutic blockade of ICs is effective in the treatment of cancers of different histologic types. However, even in responsive malignancies, not all treated patients experience meaningful clinical responses (2). Under standing mechanisms of exhaustion and, consequently, those of response to immune checkpoint blockade (ICB) is necessary for the clinical development of next generation immunotherapies and the identification of biomarkers of response.

Through analysis of transcriptomic and epigenetic profiles in murine models of chronic viral infection or cancer, a picture has emerged whereby exhausted T cells could represent a CD8^{+} T cell lineage distinct from effector or memory cells (4 6). Tissue resident memory T (Trm) cells represent, likewise, a distinct lineage of cells emerging during immune responses to infection (7 9). These cells reside in tissues, are maintained regardless of antigen persistence, and ensure protection upon local reencounter with infectious agents. In patients with cancer, CD8^{+} T cells expressing Trm markers have been identified (10, 11) and seem to overlap with exhausted T cells at tumor sites. It remains unclear, however, whether these cells represent, as in murine models of infection, CD8^{+} T cell lineages or a functional state acquired at tumor sites.

ICs can limit T cell priming and expansion by interfering with CD28 mediated costimulation and can control effector functions through the impairment of T cell receptor (TCR) complex signal ing (2, 12). PD 1 engagement leads to dephosphorylation of molecules in the TCR complex signaling pathway (13, 14), and studies have challenged this dogma and propose CD28 as the main target of PD 1 (15 17). These findings may seem at odds with the distribution of PD 1 ligands, in particular PD L1 expressed at effector sites (18),

[1]Cancer Research Center of Toulouse, INSERM UMR 1037, Toulouse, France. [2]Department of Medical Oncology, Institut Claudius Regaud, Institut Universi taire du Cancer de Toulouse, Toulouse, France. [3]Department of Pathology, Centre Hospitalier Universitaire, Institut Universitaire du Cancer de Toulouse, Toulouse, France. [4]Université Toulouse III Paul Sabatier, Toulouse, France. [5]Department of Surgery, Institut Claudius Regaud, Institut Universitaire du Cancer de Toulouse, Toulouse, France. [6]Technological Pole and BioInformatic Platform, Cancer Research Center of Toulouse, INSERM UMR 1037, Toulouse, France. [7]Department of Pathology, Institut Claudius Regaud, Institut Universi taire du Cancer de Toulouse, Toulouse, France. [8]Immune Monitoring Core Facility, Institut Claudius Regaud, Institut Universitaire du Cancer de Toulouse, Toulouse, France. [9]Department of Surgery, Centre Hospitalier Universitaire, Institut Universitaire du Cancer de Toulouse, Toulouse, France.

Note: Supplementary data for this article are available at Cancer Immunology Research Online (http://cancerimmunolres.aacrjournals.org/).

C. C. Balança, C. M. Scariata, and M. Michelas contributed equally to this article.

Corresponding Author: Maha Ayyoub, Cancer Research Center of Toulouse, INSERM UMR 1037, Toulouse 31100, France. Phone: 3 35 8274 1687; Fax: 3 35 8274 1685; E mail: maha.ayyoub@inserm.fr

and with the correlation of PD-L1 expression at tumor sites to response to PD-1/PD-L1 blockade (19). Precise assessment of PD-1 and CD28 expression in tumor-specific CD8$^+$ T cells could contribute to the clarification of the relative contribution of ICB-mediated PD-1 inhibitory signal relief on expansion and effector functions of tumor-specific T cells.

Here, in ovarian, cervical, and head and neck cancers, three epithelial malignancies exhibiting resistance to ICB, we characterized exhaustion in tumor antigen-specific CD8$^+$ T cells. We showed that along with chronic stimulation of tumor-specific T cells, IC expression was sequentially acquired, leading to a population expressing the four checkpoints PD-1, TIGIT, CTLA-4, and TIM-3, which we called quadruple positive (QP). Incremental checkpoint expression was accompanied by increased expression of Trm markers (8, 9), ectonucleotidase CD39 (20), and transcription factor TOX (21), and QP cells exhibited significant loss of CD28. QP cells were endowed with high cytotoxic potential. Circulating cancer antigen-specific T cells had a memory phenotype and expressed PD-1 and TIGIT only. At the tumor site, specific CD8$^+$ T cells acquired an exhausted Trm-like phenotype. Circulating specific PD-1^{int}CD28$^+$ T cells responded to anti-PD-1 by enhancing their proliferation in response to antigen stimulation, and specific PD-1^{hi}CD28$^{+/-}$ tumor-infiltrating lymphocytes (TIL) exhibited reversal of their functional exhaustion. QP cells were predictive of response to therapy and overall survival (OS) in patients with head and neck cancer treated by PD-1/PD-L1 blockade therapy. Our results show that the combination of proliferation/reinvigoration of circulating memory T cells that could replenish the tumor site combined with reversal of exhaustion at the tumor site contributes to PD-1/PD-L1 blockade–mediated tumor control.

Materials and Methods

Patient and healthy donor samples

Peripheral blood and tumor samples were collected from patients with head and neck, ovarian, and cervical cancer at the time of surgery for primary disease (54 patients) or for recurrence (1 patient) at the Institut Universitaire du Cancer de Toulouse–Oncopole (IUCT-O, Toulouse, France) in accordance to the Declaration of Helsinki, upon approval by the institutional review board (n°DC-2016-2656) and written informed consent. The study included: patients with stage FIGO IB1–IIIB HPV 16$^+$ and/or 18$^+$ cervical cancer with squamous and adenocarcinoma histology. Patients with stage FIGO IIIB–IVA high-grade serous or clear cell (1 patient) ovarian cancer and locally advanced, recurrent or metastatic head and neck squamous carcinoma. All patients had histologically documented tumors, were ≥18 years old at the time of study entry, were followed within a standard-of-care procedure, and had an Eastern Cooperative Oncology Group performance status of 0–2. Exclusion criteria included: known history of a positive test for hepatitis B, hepatitis C, human immunodeficiency, or hantaviruses; any condition contraindicated with blood sampling procedures; pregnancy or breast-feeding; and active, suspected, or prior documented autoimmune disease or use of immunosuppressive medication. Patients did not receive any therapy during the 3 months prior to study entry. Blood samples from 14 healthy donors were obtained from the Etablissement Français du Sang.

Plasma was harvested after heparinized whole blood centrifugation at room temperature. Peripheral blood mononuclear cells (PBMC) were isolated by density gradient sedimentation using Ficoll-Hypaque (Sigma-Aldrich). Tumor samples were rapidly transported to the research facility on ice. On arrival, samples were rinsed with PBS (Sigma-Aldrich), subsequently minced on ice to smaller pieces

(between 2–4 mm), and dissociated using C Tubes (Miltenyi Biotec) and the gentleMACS Octo Dissociator (Program MultiC01_01; Miltenyi Biotec) in Iscove's Modified Dulbecco's Medium (IMDM, Sigma-Aldrich). PBMCs and tumor single-cell suspensions were cryopreserved in FBS (Gibco) containing 10% DMSO (Sigma-Aldrich).

Pretreatment tumor biopsies used for IHC analyses were obtained from a second cohort of patients with head and neck squamous cell carcinoma receiving ICB therapy with PD-1/PD-L1–blocking agents (nivolumab, $n = 21$; pembrolizumab, $n = 1$; durvalumab, $n = 7$; and avelumab, $n = 1$) to treat locally advanced or metastatic disease. Biopsies were either obtained up to 2 months prior to the first ICB dosing (5 patients) or retrieved from archival samples (25 patients: <1 year, 8 patients; ≥1 year and <2 years, 9 patients; ≥2 years and <3 years, 4 patients; and ≥3 years and <5 years, 4 patients). Samples were handled by the Biopathological Support Platform for Clinical Studies, IUCT-O. Response to therapy was evaluated by iRECIST criteria. Progressive disease (PD) was defined as the increase of >20% of target lesions or appearance and increase in size of new lesions in at least two CT scan evaluations performed at least 4 weeks apart. Partial response (PR) was defined as a decrease of >30% in target lesions and complete response (CR) as disappearance of target and non-target lesions, both in at least two CT scans performed at least 4 weeks apart. Any response other than PD or PR/CR was considered as stable disease (SD).

Cell purification and phenotypic assessment

CD8$^+$ T cells were enriched from PBMCs or tumor single-cell suspensions by positive magnetic selection (CD8 MicroBeads, human, Miltenyi Biotec) using OctoMACS Separator and MS Columns (Miltenyi Biotec). Cells (0.5 to 1 × 10^6 CD8$^+$ T cells for PBMCs and 0.1 to 0.5 × 10^6 CD8$^+$ T cells for TILs) were assessed phenotypically by staining with mAbs specific for CD3, CD4, CD8, CD45RA, CCR7, PD-1, TIGIT, TIM-3, CD28, CD103, CD69, CD49a, and CD39, as indicated, in PBS containing 5% FBS, for 15 minutes at 4°C. For intracellular and intranuclear staining, cells were fixed and permeabilized with fixation/permeabilization buffer for 45 minutes at 4°C, and stained in permeabilization buffer for 45 minutes at 4°C with mAbs specific for CTLA-4, granzyme B, perforin, TCF-1, and TOX using the Foxp3/Transcription Factor Staining Buffer Set (eBioscience). Antibodies used are listed in Supplementary Table S1. Where indicated, CD8$^+$ T cells were stained with HLA class I dextramers containing NY-ESO-1 Peptides (Immudex) or pentamers containing CMV or EBV Peptides (ProImmune) for 30 minutes at room temperature prior to phenotypic assessment (see Supplementary Table S2 for the complete listing of multimers). Cells were analyzed using BD LSRFortessa X20, and data were analyzed using DIVA Software (BD Biosciences) or the vi-SNE Algorithm (Cytobank, Inc.).

In vitro differentiation of naïve CD8$^+$ T cells

Naïve CD8$^+$ T cells were enriched from PBMCs either by magnetic selection (Naïve CD8$^+$ T Cell Isolation Kit, human, Miltenyi Biotec) using QuadroMACS Separator and LS Columns (Miltenyi Biotec) or by total CD8$^+$ T cell–positive magnetic selection (CD8 MicroBeads, human, QuadroMACS Separator, LS Columns) followed by staining with mAbs specific for CD8, CD45RA, CCR7, and CD28, and naïve (CD45RA$^+$CCR7$^+$CD28$^+$) CD8$^+$ T cells were sorted via FACS (BD FACSAria Fusion). Antibodies are listed in Supplementary Table S1. Cells were then labeled with CFSE (5 μmol/L; eBioscience), stimulated with anti-CD3/28 beads (Miltenyi Biotec) at a bead-to-cell ratio of 1:1, and maintained in culture in the presence of recombinant human (rh)

IL2 (50 IU/mL; Miltenyi Biotec) and in the presence or absence of TGFβ (50 ng/mL; PeproTech) in IMDM (Sigma Aldrich) supplemented with 1% penicillin streptomycin Solution (Sigma Aldrich), 1% MEM Nonessential Amino Acids Solution (Invitrogen), L Glutamine (2 mmol/L, Invitrogen), and 10% human serum (Institut de Bio technologies Jacques Boy). On day 7, cells were stained with CD3 , CD8 , CD45RA , CCR7 , and CD28 specific mAbs (Supplementary Table S1) and analyzed by flow cytometry, as described above. In some experiments CD28⁻ cells were sorted from day 7 TGFβ cultures via FACS (BD FACSMelody), restimulated with anti CD3/28 beads (bead to cell ratio of 1:1) in the presence of rhIL2 (50 IU/mL) and in absence or presence of blocking PD 1 mAbs (10 µg/mL; Bristol Myers Squibb), and assessed 7 days later for CD28 expression by flow cytometry.

Droplet-based single-cell RNA-sequencing and single-cell gene expression analysis

Tumors, minced as detailed above, were transferred into digestion medium (Tumor Dissociation Kit, human, Miltenyi Biotec) and dissociated using C tubes and gentleMACS Octo Dissociator (Pro gram h TDK3, 37°C, Miltenyi Biotec). Samples were filtered using a 40 µm Nylon Mesh (BD Biosciences). Cell suspensions were then centrifuged at $300 \times g$ at 4°C for 7 minutes, the supernatant was discarded. Cell pellets were resuspended in 1 mL Red Blood Cell Lysis Buffer (Miltenyi Biotec), incubated for 10 minutes at 4°C, centrifuged, and the pellets were resuspended in PBS containing 0.04% BSA (Euromedex). CD45⁺ cells were enriched by positive magnetic selection from single cell suspensions (CD45 MicroBeads, human, Octo MACS Separator, MS Columns, Miltenyi Biotec), and cells were counted to determine the proportion of live cells. Only samples containing >90% live cells were used for single cell RNA sequencing (scRNA seq) experiments. CD45⁺ cells (2 to 4 $\times 10^5$ cells) were stained with barcoded TotalSeq A mAb (BioLegend).

Single cell libraries (3′ gene expression and antibody derived tag fractions) were generated using the Chromium Controller Instrument and Chromium Single Cell 3′ Library and Gel Bead Kit v3 according to the manufacturer's protocol (10× Genomics) with some modifications as described previously (22). To detect barcoded TotalSeq A anti bodies, an ADT library was constructed as previously described for CITE seq (22). Single cell library size and quality were confirmed on Fragment Analyzer (Agilent). KAPA Quantification Kit for Illumina platforms (Kapa Biosystems, Roche) was used to quantify library. Samples were pooled in equimolar fashion with desired proportions for the two library types (cDNA library fraction at 90% and ADT library at 10%). The libraries were sequenced on a NextSeq 550 (Illumina) in pair end sequencing 28 bp (read1) × 91 bp (read2) and a single index 8 bp in length. Raw data (FastQ files) for expression and antibody detection were computed with CellRanger 3.0 and the GRCh38 transcriptome as reference (https://support.10xgenomics.com/single cell gene expression/software/pipelines/latest/using/count). Data were then loaded in an R session with the Seurat 3.0 toolkit package involving the normalization and variance stabilization pack age sctransform (23). Samples were individually filtered using unique molecular identifier (<30′000) and percentage of mitochondrial genes (<0.25%) criteria. Using Seurat, datasets were reduced by principal component analysis using the 11 first principal components to reduce dimensionality by t distributed stochastic neighbor embedding (t SNE). A resolution parameter set the granularity at 1.2 for the clustering by the K nearest neighbor graph based clustering approach of Seurat's FindClusters function. CD8⁺ T lymphocytes were selected using Single Cell Virtual Cytometer software (https://sites.google.

com/site/fredsoftwares/products/single cell virtual cytometer) using the sum of *CD3D, CD3E,* and *CD3G* gene expression and *CD8B* gene expression. Wilcoxon *P* values for differentially expressed genes were adjusted with Benjamini Hochberg and illustrated in a volcano plot. The maturation trajectories of the selected T cells were computed with FateID as described previously (24), specifying CD8⁺ T cells in cluster 5 (**Fig. 3A**) as an endpoint. The gene set enrichment analysis of the coexpression nodes, here, taken as lists of genes, were computed with Autocompare ZE (https://sites.google.com/site/fredsoftwares/products/autocompare ze) for enrichment for gene sets from the C5 collection of gene ontology (GO) database (GSEA/MSigDB database, v6.3; refs. 25 27). ScRNA seq data have been deposited in NCBI's Gene Expression Omni bus (GEO; ref. 28) and are accessible through GEO series accession number GSE148162.

T-cell functional assessment

CD8⁺ T cells isolated from tumor single cell suspensions were stimulated with phorbol 12 myristate 13 acetate (PMA, 100 ng/mL; Sigma Aldrich) and ionomycin (1 µg/mL; Sigma Aldrich) or plate bound anti CD3 (1 µg/mL; eBioscience) in the presence of anti CD107a (Supplementary Table S1) for 6 hours in IMDM supplemented as described above. Brefeldin A (10 µg/mL; Sig ma Aldrich) was added 1 hour after the beginning of the incuba tion. Cells were then stained with mAbs, as described above, specific for CD3, CD4, CD8, and PD 1, and cytokine production was assessed by intracellular staining using IFNγ and TNFα specific mAbs (Supplementary Table S1). The cells were analyzed by flow cytometry (BD LSRFortessa X20).

For the assessment of NY ESO 1 specific cells, CD8⁺ T cells were magnetically sorted from PBMCs and tumor single cell suspensions, as already described, from patients with ovarian cancer exhibiting antibody responses to NY ESO 1. Antibody responses to NY ESO 1 were assessed in patient plasma by ELISA, as described previously (29) and detailed hereafter. Eighteen overlapping 20 to 24 amino acid long peptides encompassing the full length NY ESO 1 sequence (25 µg/mL each in PBS; Peptide 2.0 Inc) were coated on Nunc MaxiSorp Flat Bottom ELISA Plates (Thermo Fisher Scientific) overnight at 4°C. Plates were then washed with PBS, 0.005% Tween (Sigma Aldrich), incubated for 2 hours at 37°C with blocking buffer (PBS, 2% BSA), and washed with PBS, 0.005% Tween. Plasma (diluted 1/100 in blocking buffer) was incubated for 2 hours at room temperature and washed using the same buffer. Plates were then incubated for 1 hour at room temperature with goat anti human IgG secondary antibodies (Sigma Aldrich; 1 µg/mL in blocking buffer) and washed. ELISA was developed using the Alkaline Phosphatase Yellow (pNPP) Liquid Substrate System for ELISA (Sigma Aldrich). Isolated CD8⁺ T cells (20,000 to 150,000 CD8⁺ T cells from TILs and 2 to 5 × 10⁵ CD8⁺ T cells from PBMCs, per well) were stimulated with NY ESO 1 peptides (1 µmol/L; Peptide 2.0 Inc) in the presence of autologous CD14⁺ cells sorted from PBMCs by positive magnetic selection (CD14 MicroBeads, human, OctoMACS Separator and MS Columns, Miltenyi Biotec) at a 1.5 to 1 CD14⁺ to CD8⁺ cell ratio, and rhIL2 (50 IU/mL) in the absence or presence of PD 1 blocking mAb (10 µg/mL) in IMDM supplemented as above. Day 5 7 cultures were either stained with HLA class I dextramers containing NY ESO 1 peptides and with anti CD8 or stimulated or not with NY ESO 1 peptides (1 µmol/L) and assessed for IFNγ and TNFα production by intracellular staining, as detailed above.

Quantitative multiplex IHC

Sequential chromogenic IHC was performed on 4 µm thick tumor tissue sections based on the protocol described by Glass and colleagues

with some modifications (30) using mAbs listed in Supplementary Table S3. Briefly, slides were dewaxed, subjected to heat mediated antigen retrieval (Target Retrieval Buffer pH9 K800021 2, Dako Agilent), and immunostained using 3 amino 9 ethylcarbazole (AEC, Dako Agilent) as chromogen according to the manufacturer's recommendations. To preserve antigens, slides were then mounted with an Aqueous Mounting Medium (Dako Agilent) containing 60% glycerol, 40% distilled H_2O, and 10% (w/w) saturated sucrose H_2O (584 mmol/L; ref. 30) and scanned using Pannoramic 250 Flash III Scanner (3DHISTECH Ltd.). After scanning, AEC and antibodies were removed. Slides were unmounted and washed with distilled H_2O before being discolored with increasing gradients of absolute ethanol (70% 90%, Sigma Aldrich) according to the SIMPLE1 method (30), and rinsed with distilled H_2O. Antibody stripping was performed by incubation of slides for 30 minutes at 56°C in a freshly prepared stripping buffer [1% SDS (w/v, Sigma Aldrich), 0.2 mol/L Tris HCl pH 6.8 (CliniScience), and 0.1 mol/L β Mercaptoethanol (Sigma Aldrich) in distilled H_2O; ref. 31], followed by rinsing with distilled H_2O for 45 minutes. The entire sequence was repeated for each antigen assessed.

For each case, at least one region of interest (ROI) of 5,000 × 5,000 pixels (1,200 μm²) was selected and extracted from each of the virtual slides using ImageScope (Aperio Leica Biosystems). Extracted images were registered using ImageJ "Register Virtual Stack Slices" plugin and color deconvoluted using FIJI (1.52n). Nuclei segmentation was per formed with ILASTIK software. Cell identification, staining evalua tion, and results export in csv format was performed using CellProfiler software. Pathologists defined fluorescence value for each cell and each marker in the ROI and the positivity thresholds for each marker. These thresholds were used for the determination of CD3$^+$CD8$^+$ (CD8$^+$ T cells) and CD3$^+$CD8$^+$TIM 3$^+$ (TIM 3$^+$CD8$^+$ T cells) cell proportions among all nuclei. The median of CD3$^+$CD8$^+$ and CD3$^+$CD8$^+$TIM 3$^+$ cell proportions in all patients was used as cutoff to define high (≥median) and low (<median) infiltration for each population.

In vivo experiments

Female C57BL/6 mice, 7 weeks old, were purchased from Janvier Labs. Experimental protocols were approved by regional Ethic Committee of Toulouse Biological Research Federation (C2EA 01, FRBT) and by the French Ministry for Higher Education and Research. The European directive 2010/63/EU was followed for guidelines on animal welfare. TC1 cells expressing the HPV 16 E6 and E7 proteins were developed in the laboratory of T.C. Wu (Department of Pathology, School of Medicine, Johns Hopkins University, Baltimore, MD). Cells were cultured in complete RPMI1640 Medium (Life Technologies) for 2 6 passages and tested negative for *Mycoplasma*.

When 8 weeks old, mice were anesthetized by intraperitoneal injection of anesthetic mix [10 μL/kg; made up of ketamine (100 mg/kg) and xylazine (10 mg/kg); Centravet], and implanted in the oral cavity (intracheek) with 3 × 10^4 TC1 cells suspended in a final volume of 10 μL of PBS using a Hamilton syringe and 30G needle. At day 10 and 18, mice were sacrificed by intraperitoneal injection of anesthetic mix (10 μL/kg), followed by vertebral dislocation. Oral tumors were harvested, cut in pieces, and enzymatically digested using the Mouse Tumor Dissociation Kit (Miltenyi Biotec), C tubes, and gentleMACS Octo Dissociator (program 37C m TDK 1). Digestion was followed by filtration through a 70 μm cell strainer. Cells were resuspended in PBS containing 2% FBS, anti CD16/CD32 (Supple mentary Table S1), and 1:1,000 Fixable Viability Dye Stain 700 (BD Biosciences). Staining with mAbs specific for cell surface markers

(Supplementary Table S1) and flow cytometry analyses were per formed as described above for human samples.

Statistical analyses

Normality was assessed using the Shapiro Wilk test. For normally distributed values, the t test was used for paired or unpaired data. When the values were not normally distributed, the comparison of variables was performed with Wilcoxon or Mann Whitney test for paired and unpaired data, respectively. Lines and error bars in scatter plots represent mean ± SD. For correlations, Pearson test was used to compare variables. For OS analyses, ICB treated patients were sub divided into two groups according to high (≥median) and low (<median) tumor infiltration by CD8$^+$ T cells or TIM 3$^+$CD8$^+$ T cells, Kaplan Meier curves were plotted, and P values determined by log rank test. Results of statistical analyses are annotated as follows in figures: ns, not significant ($P \geq 0.05$); *, $P < 0.05$; **, $P < 0.01$; ***, $P < 0.001$; ****, $P < 0.0001$. All analyses were performed with GraphPad Prism 7 software.

Results

IC expression defines six tumor-infiltrating CD8$^+$ T-cell populations

We assessed *ex vivo* CD8$^+$ ovarian, cervical, and head and neck cancer (HNC) TILs for PD 1, TIGIT, CTLA 4, and TIM 3. Each of the four checkpoints was expressed in the three tumor types (**Fig. 1A**; Supplementary Fig. S1A). PD 1 was on average expressed in a higher proportion of cells, followed by TIGIT, CTLA 4, and TIM 3. Although TIGIT could be expressed both independently and alongside PD 1 (Supplementary Fig. S1A, left contour plots), CTLA 4 and TIM 3 expression appeared systematically associated to that of PD 1 (Sup plementary Fig. S1A, center and right contour plots, respectively). This was supported by correlation analyses, which revealed significant positive correlation between the proportion of PD 1 expressing cells and those expressing CTLA 4 and TIM 3 but not TIGIT (Supple mentary Fig. S1B). We then analyzed CTLA 4 and TIM 3 expression in cells expressing or not PD 1 and TIGIT (**Fig. 1B**). The majority of PD 1$^-$TIGIT$^-$ cells did not express CTLA 4 and TIM 3, which we named "quadruple negative" (QN). PD 1$^+$TIGIT$^-$ and PD 1$^-$TIGIT$^+$ cells did not express CTLA 4 and TIM 3. We named these cells "PD 1 single" (PD 1s) and "TIGIT single" (TIGITs), respectively. PD 1$^+$TIGIT$^+$ cells could be divided into three popula tions according to CTLA 4 and TIM 3 expression: (i) expressed neither CTLA 4 nor TIM 3; (ii) expressed CTLA 4 only; and (iii) expressed both, called "double positive" (DP), "triple positive" (TP), and "quadruple positive" (QP), respectively (**Fig. 1B**). Among the 16 possible coexpression profiles (**Fig. 1B**, bottom), the six populations described above were the most frequently and consistently detected in the three tumor types. The QP population showed the highest inter individual variation (range 0.7% 62%, median 20.69%). Similar anal yses from circulating memory/effector CD8$^+$ T cells from healthy individuals and patients with cancer showed that only QN, PD 1s, TIGITs, and DP populations were detectable, implying that acquisition of CTLA 4 and TIM 3 expression takes place *in situ* (Supplementary Fig. S2).

In CD8$^+$ TILs, we found that cells expressing both PD 1 and TIGIT exhibited higher staining intensity for both markers compared with cells expressing each alone (**Fig. 1B**; Supplementary Fig. S1A, left contour plots). Analysis of mean fluorescence intensity (MFI) showed that PD 1 MFI incrementally and significantly increased in parallel to the number of expressed ICs in each PD 1$^+$ population (**Fig. 1C**, left).
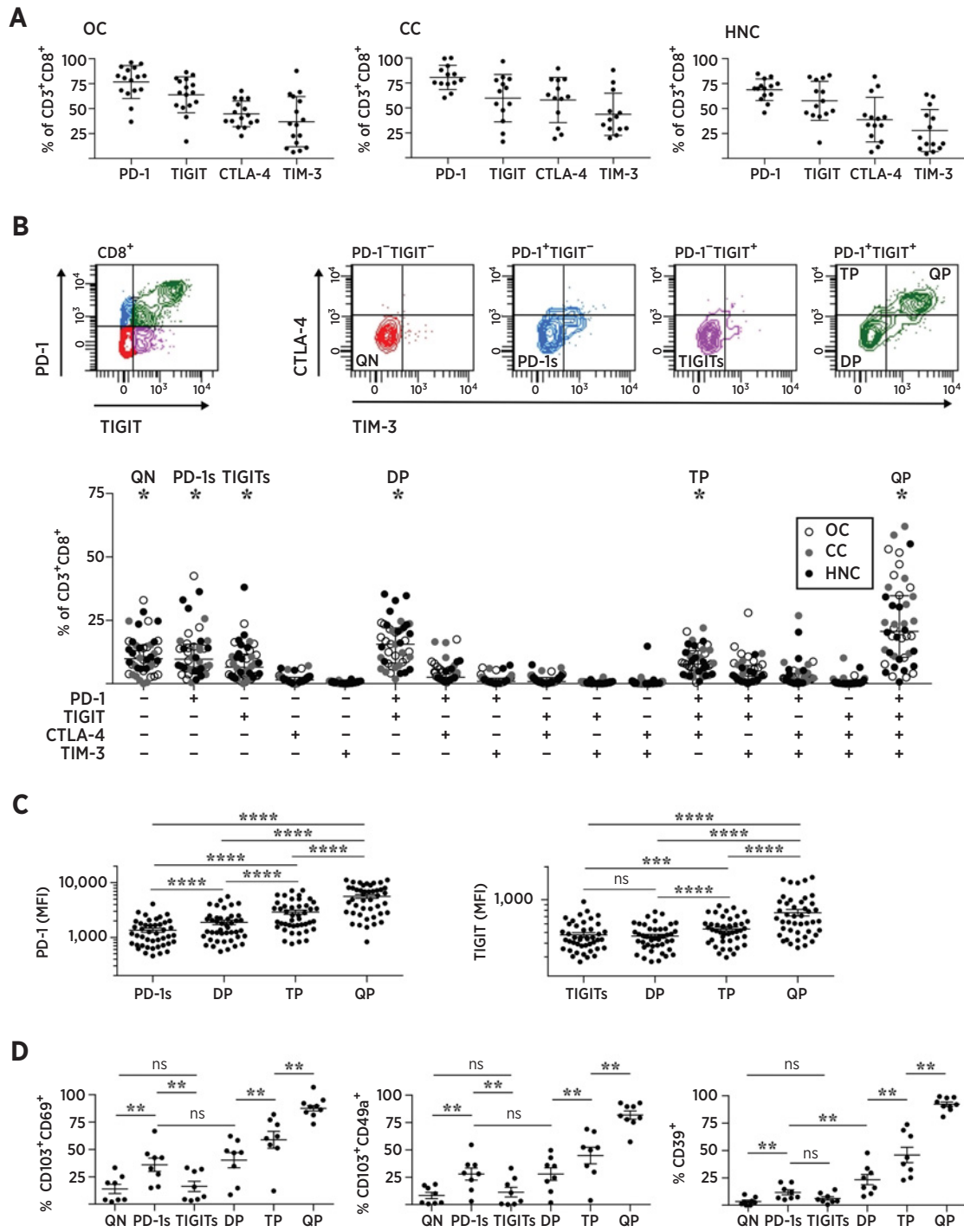
Figure 1.
Coexpression of ICs defines six tumor infiltrating CD8$^+$ T cell populations. CD8$^+$ TILs were stained *ex vivo* with mAbs specific for CD3, CD8, PD 1, TIGIT, CTLA 4, TIM 3, CD103, CD69, CD49a, and CD39 and analyzed by flow cytometry. **A,** Proportion of CD8$^+$ TILs expressing PD 1, TIGIT, CTLA 4, or TIM 3 for three malignancies (ovarian cancer, OC, $n = 17$; cervical cancer, CC, $n = 12$; and HNC, $n = 15$). Nineteen independent experiments. Examples of contour plots are shown in Supplementary Fig. S1A. **B,** Representative contour plots showing CD8$^+$ T cell CTLA 4 and TIM 3 expression (top right) from gated PD 1 TIGIT , PD 1$^+$TIGIT , PD 1 TIGIT$^+$, and PD 1$^+$TIGIT$^+$ populations (top left). Data corresponding to the proportion of each of the 16 combinations of IC expression are summarized (numbers of samples are as in **A**; bottom). Median proportions, among CD8$^+$ TILs, for six subpopulations (*) was >5%. **C,** MFI of PD 1 and TIGIT in PD 1$^+$ and TIGIT$^+$ cells, respectively, among CD8$^+$ TIL subpopulations. **D,** Proportion of CD103$^+$CD69$^+$, CD103$^+$CD49a$^+$, and CD39$^+$ cells among the six CD8$^+$ TIL subpopulations identified in **B** (ovarian cancer, $n = 5$; cervical cancer, $n = 2$; and HNC, $n = 2$; five independent experiments). Examples of dot plots and histogram plots are shown in Supplementary Fig. S4. The Wilcoxon test was used to compare variables (ns, not significant; **, $P < 0.01$; ***, $P < 0.001$; ****, $P < 0.0001$).

A similar pattern was observed for TIGIT, although the MFI did not vary significantly between the TIGITs and DP populations (**Fig. 1C**, right).

Altogether, these analyses revealed a conserved pattern of IC expression in the three tumor types, which defined six CD8$^+$ T cell populations. Analysis of PD 1 and TIGIT suggested an increase in their expression alongside a possible sequential acquisition of CTLA 4 followed by TIM 3. In an orthotopic mouse model of HNC, PD 1 MFI at the tumor site was, likewise, increased in PD 1$^+$CD8$^+$ T cells coexpressing TIM 3 compared with those expressing PD 1 only (Supplementary Fig. S3). In further support of the sequential acqui sition model, the proportion of PD 1$^+$TIM 3$^+$ cells was higher at day 18 than day 10 tumors (Supplementary Fig. S3A).

IC acquisition is paralleled by Trm markers and CD39 expression, and CD28 loss

We assessed the expression of Trm markers, CD103, CD69, and CD49a (8), and CD39, also expressed in CD103$^+$CD8$^+$ T cells at tumor sites (20), in the six CD8$^+$ T cell populations identified (**Fig. 1D**; Supplementary Fig. S4). Trm markers and CD39 were absent or expressed in low proportions in QN and TIGITs populations. Their proportions were significantly higher among PD 1s cells versus QN cells. Whereas no difference in Trm marker expression was detected between PD 1s and DP cells, CD39 expression was significantly higher in the DP population. Expression of all markers significantly increased within the TP population relative to DP cells and was further increased in the QP population. These data further supported the serial acqui sition pattern of ICs by CD8$^+$ T cells at the tumor site.

The sequential acquisition of ICs is indicative of sustained T cell stimulation and could imply disparities in the differentiation stage between cells expressing few or several ICs. Assessment of the differ entiation stage of tumor infiltrating CD8$^+$ T cells showed that the population was homogenous and mostly composed of effector mem ory cells (CD45RA$^-$CCR7$^-$; **Fig. 2A**). Effector memory cells are composed of cells expressing CD28 and cells in a more advanced differentiation stage that are CD28$^-$ (32). We found that effector memory TILs contained a significantly lower proportion of CD28$^+$ cells versus circulating effector memory cells (**Fig. 2B**; Supplementary Fig. S5A). The CD28$^-$ population at the tumor site was enriched in cells expressing the four ICs (**Fig. 2C**), suggesting loss of CD28 alongside IC acquisition. Analysis of CD28 expression according to IC coexpression profiles defined above showed significant loss in CD28 expression in the QP population (**Fig. 2D**; Supplementary Fig. S5B). Unsupervised integration of flow cytometry data using vi SNE (33) identified a QP population expressing Trm markers and CD39 while being CD28$^-$ (**Fig. 2E**).

We sought to identify tumor related factors underlying CD28 loss. The QP population was characterized by CD103 and high PD 1 expression, two features that depend on TGFβ signaling (9, 34). We found that *in vitro* stimulation of naïve CD8$^+$ T cells in the presence of TGFβ led to an enhanced loss of CD28 (**Fig. 2F**; Supplementary Fig. S5C). This was not simply due to progression in the differentiation stage as TGFβ led to delayed differentiation (**Fig. 2G**). Loss of CD28 could not be recovered by PD 1 blockade of stimulated CD28$^-$ cells, isolated from TGFβ cultures (Supplementary Fig. S5D).

ScRNA-seq reveals active immune pathway signatures in IC-positive CD8$^+$ T cells

To characterize the QP population, we performed scRNA seq of total tumor infiltrating CD45$^+$ cells isolated from 2 patients with HNC. A total of 17.9% were identified as CD8$^+$ T cells and their clustering identified 11 clusters (**Fig. 3A**, top left). Clusters 0, 1, 4, 5, and 9 showed the highest *HAVCR2* (TIM 3) expression (**Fig. 3A**). *CTLA4* was found in the same clusters as well as in clusters 7 and 3. Expression of *TIGIT* was found in most clusters, although it was more frequent in clusters expressing *HAVCR2*. *PDCD1* (PD 1) was also detected in most clusters, although the frequency of positive cells was lower than expected, presumably owing to low levels or low detection of this specific mRNA. Clusters 1, 4, 5, and 9 contained the highest proportion of cells exhibiting a QP profile and also contained cells expressing *ITGAE* (CD103), *ITGA1* (CD49a), and *ENTPD1* (CD39; **Fig. 3A**). We then performed differential mRNA expression analysis between regrouped clusters 1, 4, 5, and 9 and all other clusters. We identified 761 genes with higher expression in the QP clusters and 94 with higher expression in the other clusters (**Fig. 3B**). Genes shown in green in the volcano plot (**Fig. 3B**) correspond to markers we had used to characterize these populations (**Fig. 2E**), and their expression (**Fig. 3C**) confirmed that clusters on the right side of the t SNE plot were most representative of the QP population.

Consistent with IC expression, QP clusters expressed *TOX*, which encodes a DNA binding protein involved in T cell exhaustion (**Fig. 3B** and **C**; ref. 21). Differential analysis identified a clear cytotoxicity signature in QP clusters, including granzymes A, B, and H (*GZMA, GZMB,* and *GZMH,* respectively), perforin (*PRF1*), and granulysin (*GNLY*; **Fig. 3B** and **C**). Twenty one transcription factors were previously identified as being key for memory CD8$^+$ T cell develop ment and function (35). Of those, seven were differentially expressed in our analysis with SOX 4 (*SOX4*), Class E bHLHe40 (*BHLHE40*), PRDM1, and RUNX2 being more expressed in the QP clusters and KLF2, T cell factor 1 (TCF 1, *TCF7*), and BACH2 in the other clusters (**Fig. 3B** and **D**). Expression of SOX 4 is promoted by TGFβ (36) and induces CXCL13 production by CD4 T cells (37). *CXCL13* was more expressed in QP clusters (**Fig. 3B** and **D**). Among transcription factors that were less expressed in QP clusters, KLF2 has been shown to be downregulated in Trm cells, leading to downmodulation of S1PR1 expression (7). Differential analysis showed lower *S1PR1* expression in QP clusters (**Fig. 3B** and **D**). TCF 1 (*TCF7*) was also less expressed in QP clusters. In addition to *TCF7* and *CD28*, other early memory T cell markers were also less expressed in QP clusters, including *CCR7* and *IL7R* (**Fig. 3B** and **D**). Differential analysis also revealed higher expression of the chemokine receptor gene *CXCR6* in QP clusters (**Fig. 3B** and **D**).

We then computed a pseudotime maturation trajectory anchored by cluster 5 cells as an endpoint (**Fig. 3A**). Visualizing gene expression in cells along this trajectory showed *TCF7, IL7R,* and *CCR7* expression in cells clustered at early stages of the maturation trajectory, whereas cells expressing ICs, Trm and cytotoxicity markers, as well as *CXCL13* and *CXCR6*, clustered at later stages of the trajectory (**Fig. 3E**). Respective expression profiles of chronologically ordered cells were then Z score transformed to reveal putative temporally restricted gene sets. This identified 21 gene expression nodes, which were then analyzed for enrichment of signatures from the C5 collection of GO database. This unveiled the prominence of translational signatures during the earliest maturation stages (nodes 16 20), followed in the latest stages by signatures of immune responses (nodes 1 3; Supplementary Fig. S6). These results revealed that exhausted Trm like QP cells are the most immunologically active CD8$^+$ T cells at the tumor site.

IC QP CD8$^+$ T cells are tumor-specific and respond to PD-1 inhibition

We next assessed QP cell effector function, antigen specificity, and response to PD 1 inhibition. Tumor infiltrating CD8$^+$ T cells showed
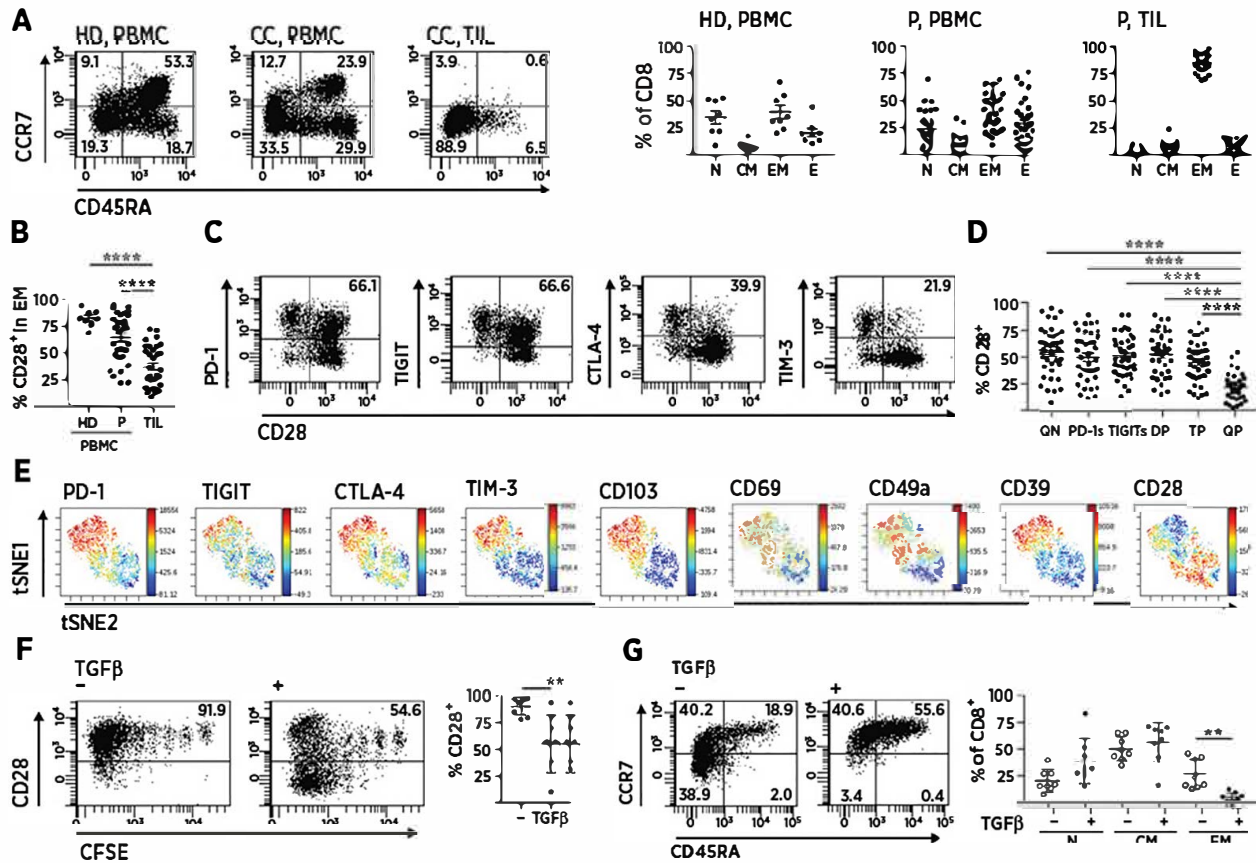
Figure 2.

TGFβ mediated loss of CD28 in QP CD8$^+$ TILs. **A,** Expression of CCR7 versus CD45RA *ex vivo* in CD8$^+$ T cells from 1 healthy donor (HD) and 1 patient with cervical cancer (CC; left). Proportions of naïve (N), central memory (CM), effector memory (EM), and effector (E) CD8$^+$ T cells are summarized (right). Healthy donor PBMCs, n = 8; patient (P) PBMCs (ovarian cancer, n = 12; cervical cancer, n = 9; and HNC, n = 11); and TILs (ovarian cancer, n = 17; cervical cancer, n = 11; and HNC, n = 9). Twenty independent experiments. **B,** Proportion of CD28$^+$ cells among EM CD8$^+$ T cells is summarized. Histogram plots are shown in Supplementary Fig. S5A. Healthy donor PBMCs, n = 8; patient PBMCs (ovarian cancer, n = 13; cervical cancer, n = 9; and HNC, n = 11); and TILs (ovarian cancer, n = 16; cervical cancer, n = 8; and HNC, n = 7). Eighteen independent experiments. **C,** Expression of CD28 versus PD 1, TIGIT, CTLA 4, and TIM 3 in CD8$^+$ T cells from 1 representative ovarian cancer patient's TILs. **D,** Proportion of CD28$^+$ cells in the six CD8$^+$ TIL subpopulations defined as in **Fig. 1B.** Ovarian cancer, n = 16; cervical cancer, n = 10; and HNC, n = 11. Ten independent experiments. CD28 staining is shown in Supplementary Fig. S5B. **E,** t SNE plots of flow cytometry data of CD8$^+$ TILs (ovarian cancer, n = 1; cervical cancer, n = 1; and HNC, n = 1). **F** and **G,** Naïve CD8$^+$ T cells were sorted from PBMCs of healthy donors (Supplementary Fig. S5C), CFSE labeled, and stimulated with anti CD3/CD28 in the absence ( ) or presence (+) of TGFβ. Day 7 cultures were stained for CD3, CD8, CCR7, CD45RA, and CD28 and analyzed by flow cytometry (healthy donors, n = 8; three independent experiments). **F,** CD28 versus CFSE staining in CD8$^+$ T cells for 1 healthy donor (left); the proportion of CD28$^+$ cells is summarized (right). **G,** CCR7 versus CD45RA expression in CD8$^+$ T cells (left); the proportion of naïve, central memory, and effector memory cells is summarized for each stimulation condition (right). P values were calculated using Mann Whitney test (**B**), Wilcoxon test (**D–G**), and paired t test (**F**; **, $P < 0.01$; ****, $P < 0.0001$).

progression in TOX expression along IC acquisition (Fig. 4A and B; Supplementary Fig. S7A and S7B). An opposite pattern was observed for the expression of TCF 1 (Supplementary Fig. S8A). Absence of TCF 1 in late stage populations at the tumor site was in agreement with its progressive loss along differentiation in circulating CD8$^+$ T cells (Supplementary Fig. S8B and S8C). Expression of granzyme B and perforin, inferred from scRNA seq analyses, was also confirmed at the protein level. The proportion of cells expressing both proteins was higher in the QP population than in other CD8$^+$ TILs (Fig. 4A and B). This was consistent with their CD28$^-$ phenotype indicating advanced differentiation (32).

To validate the effector potential of QP cells, we stimulated tumor infiltrating CD8$^+$ T cells with PMA/ionomycin (i.e., bypassed prox imal TCR signaling and IC inhibition). PMA/ionomycin stimulation perturbed, in some samples, TIGIT, CTLA 4, and TIM 3 expression but not that of PD 1. We, therefore, analyzed cytokine production and

CD107a surface expression in CD8$^+$ populations defined by PD 1 expression (Fig. 4C). PD 1$^-$ cells encompassed the QN and TIGITs populations, PD 1^{int} corresponded to PD 1s and DP populations, and PD 1^{hi} represented the TP and QP populations (Fig. 1B and C). Our data showed that PD 1^{hi} cells were able to release cytotoxic granules and produce cytokines (Fig. 4D and E). Compared with the two other populations, PD 1^{hi} cells encompassed fewer polyfunctional cells, that is, able to produce both IFNγ and TNFα, and more IFNγ$^+$TNFα$^-$ cells (Fig. 4E), a feature that has been associated with exhaustion (38). Accordingly, upon anti CD3 instead of PMA/ionomycin stimulation, PD 1^{hi} cells comprised fewer cytokine producing cells than less exhausted, PD 1$^-$ and PD 1^{int}, populations (Fig. 4F).

NY ESO 1, a cancer testis antigen expressed in ovarian cancer, induces both antibody and T cell responses (29). Several NY ESO 1 derived CD8$^+$ T cell epitopes are presented by frequently expressed HLA class I alleles (39). Within the ovarian cancer cohort, we identified
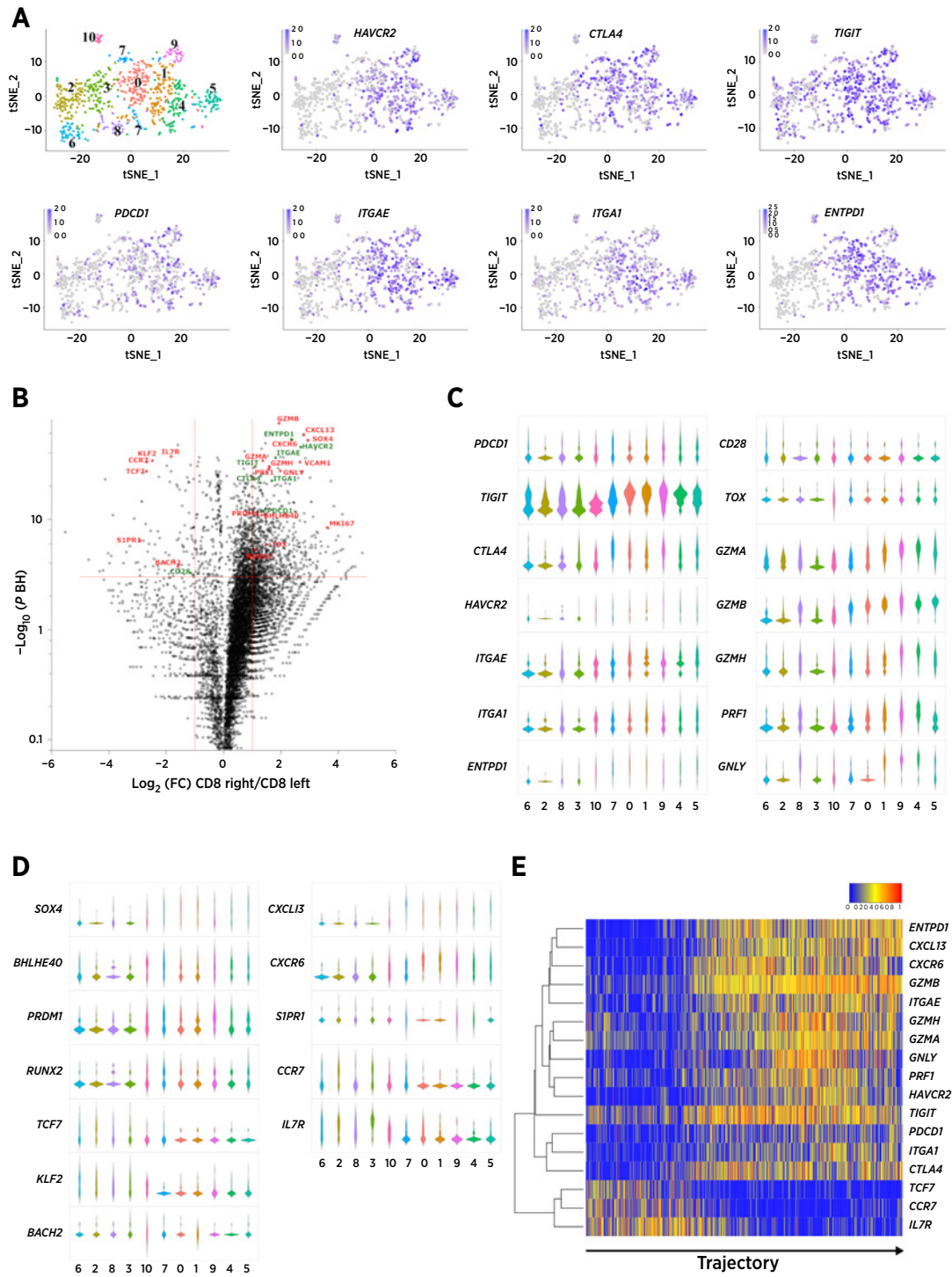
Figure 3.
ScRNA seq reveals cytotoxic and active immune pathway signatures in IC positive CD8 T cells. CD45^{+} cells isolated *ex vivo* from two HNC specimens were subjected to scRNA seq. **A,** t SNE plots of 752 CD8^{+} T cells (top left) color coded by their associated cluster and t SNE plot color coded for expression (gray to blue) of *HAVCR2, CTLA4, TIGIT, PDCD1, ITGAE, ITGA1,* and *ENTPD1*. **B,** Differential analysis of scRNA seq data from clusters 1, 4, 5, and 9 versus those from the remaining clusters. Genes encoding markers used above to characterize CD8^{+} TILs are shown in green, and part of the new genes identified with significant differential expression are shown in red. **C** and **D,** Violin plots showing the expression of selected genes in the 11 clusters. *x* axes indicate cluster number. **E,** FateID heatmap based on the trajectory identified by pseudotime analysis (Supplementary Fig. S6).
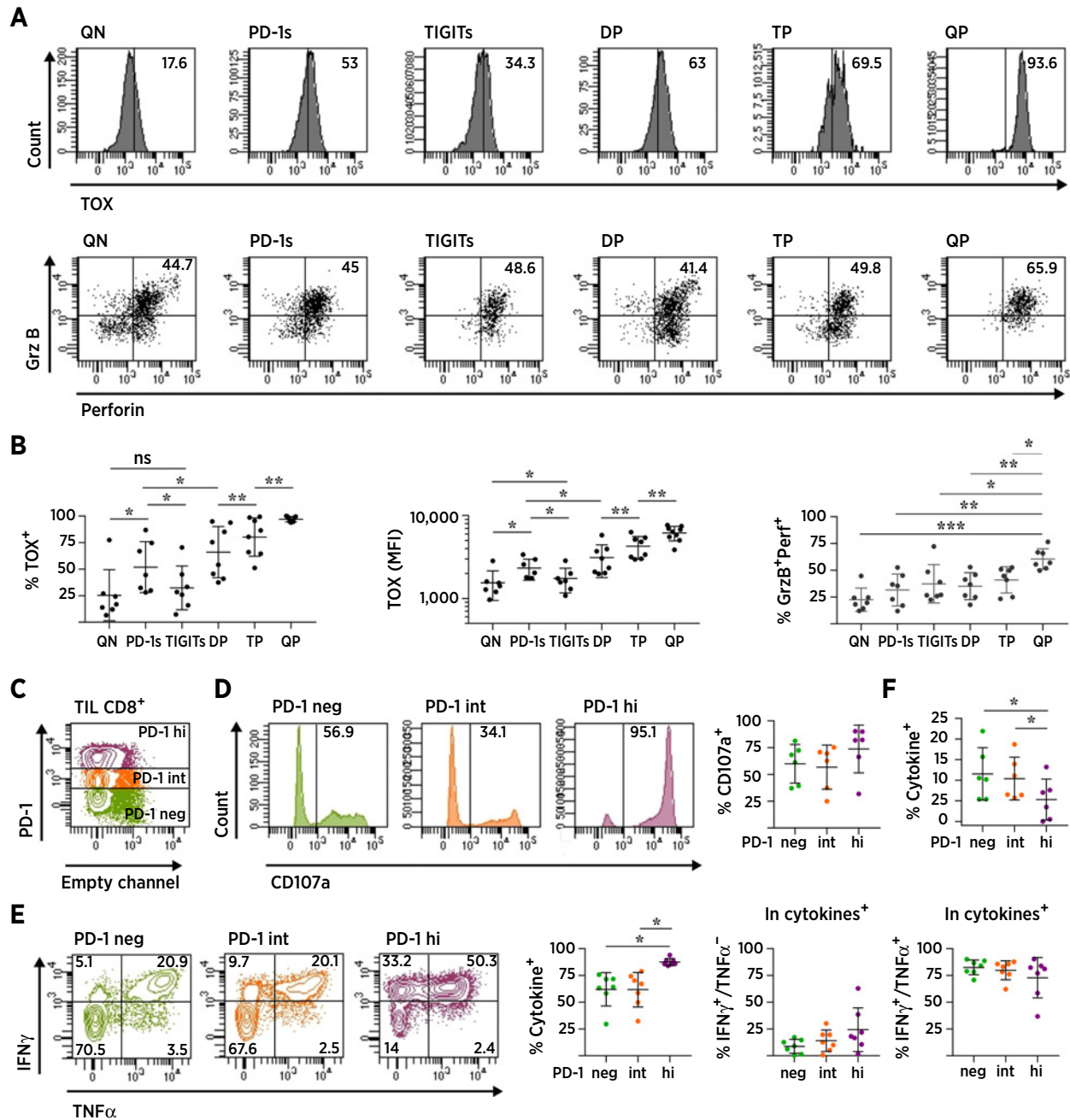
Figure 4.
IC QP cells retain effector potential. **A** and **B,** CD8^{+} TILs were stained *ex vivo* with mAbs specific for CD3, CD8, PD 1, TIGIT, CTLA 4, TIM 3, TOX, granzyme B (GrzB), and perforin (Perf) and analyzed by flow cytometry. **A,** Histograms showing TOX expression (top) and dot plots of granzyme B versus perforin expression (bottom) in the indicated CD8^{+} TIL subpopulations. The cutoff for TOX staining was determined on the basis of TOX staining in CD8^{+} T cells from PBMCs (Supplementary Fig. S7A). **B,** Proportion of TOX^{+} cells (left), MFI of TOX staining in total cells in each population (middle; ovarian cancer, $n = 4$; cervical cancer, $n = 3$; and HNC, $n = 2$; two independent experiments), and proportion of GrzB^{+}Perf^{+} cells (right; ovarian cancer, $n = 4$; cervical cancer, $n = 2$; HNC, and $n = 1$; four independent experiments) in CD8^{+} TIL subpopulations are summarized. CD8^{+} TILs were stimulated *ex vivo* with PMA/ionomycin (two independent experiments; **C–E**) or anti CD3 (two independent experiments; **F**) in the presence of anti CD107a and brefeldin A for 6 hours. Cells were then stained for CD3, CD8, PD 1, IFNγ, and TNFα and analyzed by flow cytometry. **C,** Gating strategy based on PD 1 expression (PD 1[neg], green; PD 1[int], orange; and PD 1[hi], purple; maintained throughout figure). **D,** Histogram plots showing surface CD107a expression gated on the indicated populations (left). Proportions of CD107a^{+} cells in each population are summarized (right; ovarian cancer, $n = 5$ and HNC, $n = 1$). **E,** IFNγ versus TNFα staining gated on the indicated populations (left). The proportion of total cytokine[+] (IFNγ and/or TNFα) cells, as well as those of IFNγ single positive and IFNγ/TNFα double positive cells among total cytokine^{+} cells are summarized for each CD8^{+} TIL subpopulation (right; ovarian cancer, $n = 6$ and HNC, $n = 1$). **F,** Proportion of total cytokine^{+} (IFNγ and/or TNFα) cells among each CD8^{+} TIL subpopulation (cervical cancer, $n = 2$ and HNC, $n = 4$). P values were determined using the Wilcoxon test (**B**, %TOX^{+} and TOX MFI; **E**) or paired t test (**B**, %GrzB/Perf[+]; **F**; ns, not significant; *, $P < 0.05$; **, $P < 0.01$; ***, $P < 0.001$).
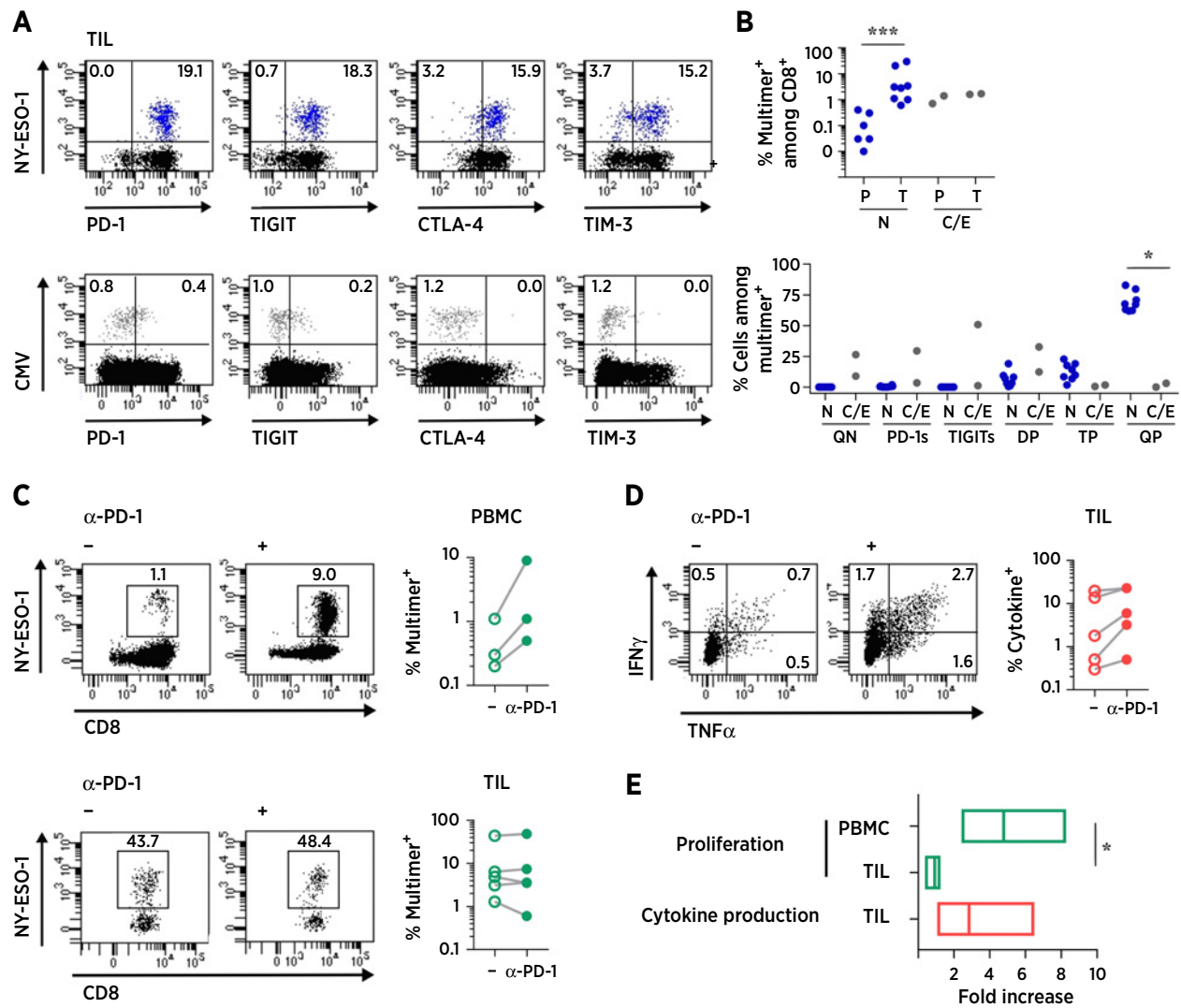
Figure 5.
IC QP cells encompass tumor specific cells and respond to PD 1 inhibition. **A** and **B,** CD8$^+$ TILs were stained *ex vivo* with HLA class I multimers harboring NY ESO 1, cytomegalovirus (CMV), or Epstein Barr virus (EBV) epitopes and with mAbs specific for CD3, CD8, PD 1, TIGIT, CTLA 4, and TIM 3 and analyzed by flow cytometry. **A,** NY ESO 1 multimer (NY ESO 1, top) and CMV multimer (CMV, bottom) staining versus PD 1, TIGIT, CTLA 4, and TIM 3 expression gated on CD8$^+$ T cells from representative patients with ovarian cancer. NY ESO 1$^+$ cells shown in blue and CMV$^+$ in gray. **B,** Summary of the proportions of NY ESO 1 [N; PBMC (P), ovarian cancer, $n = 6$; TIL (T), ovarian cancer, $n = 8$) and CMV or EBV (C/E; PBMC and TIL: ovarian cancer, $n = 1$, HNC, $n = 1$) multimer$^+$ cells among CD8$^+$ T cells isolated from PBMCs and TILs (top, 13 independent experiments). Examples of staining of circulating CD8$^+$ T cells are shown in Supplementary Fig. S9A. Summary of the proportions of QN, PD 1s, TIGITs, DP, TP, and QP cells among NY ESO 1 and CMV or EBV multimer$^+$ CD8$^+$ TILs. NY ESO 1$^+$ cells shown in blue (bottom, four independent experiments). **C** and **E,** CD8$^+$ T cells isolated from PBMCs and TILs of NY ESO 1 seropositive patients with ovarian cancer were stimulated *in vitro* with NY ESO 1 peptides and autologous CD14$^+$ cells in the absence ( ) or presence (+) of blocking anti PD 1. **C,** Day 5 to 7 cultures were stained with NY ESO 1 multimers and anti CD8 and analyzed by flow cytometry (seven independent experiments). Representative dot plots (left) and the proportion of multimer$^+$ cells among CD8$^+$ T cells (right) are shown (top, PBMCs, $n = 3$; bottom, TILs, $n = 5$). Connected points indicate the same patient sample. **D,** Day 7 TIL cultures restimulated with NY ESO 1 peptides and tested for IFNγ and TNFα production by intracellular cytokine staining (four independent experiments). Representative dot plots (left) and the proportion of cytokine$^+$ cells among CD8$^+$ T cells in each culture condition (right) are shown ($n = 5$). Connected points indicate the same patient sample. **E,** Floating bars (min to max) represent fold increase in the proportion of multimer$^+$ cells (proliferation) and of cytokine$^+$ cells in CD8$^+$ T cells stimulated in presence of anti PD 1 compared with those stimulated in absence of anti PD 1. *P* values were calculated using Mann Whitney test (**B**) and unpaired *t* test (**E**; *, *P* < 0.05; ***, *P* < 0.001).

patients with serologic responses to the antigen, indicative of an ongoing T cell response (29). We used HLA class I/NY ESO 1 fluo rescent multimers to detect antigen specific T cells in these patients. The proportion of antigen specific T cells was higher in CD8$^+$ cells isolated from TILs than from PBMCs, suggesting that they were preferentially attracted, proliferated, and/or were retained at tumor

sites (**Fig. 5A** and **B**; Supplementary Fig. S9A). Similar proportions of CD8$^+$ T cells specific for chronic viruses were detected in PBMCs and TILs (**Fig. 5A** and **B**; Supplementary Fig. S9A), further confirming the specific *in situ* accumulation of tumor specific T cells. NY ESO 1 specific T cells in the periphery expressed PD 1 and TIGIT, both with intermediate MFIs, whereas they had a QP phenotype at the tumor site

(**Fig. 5A** and **B**; Supplementary Fig. S9). In contrast, bystander virus specific T cells never acquired the QP phenotype at the tumor site (**Fig. 5A** and **B**; Supplementary Fig. S9). NY ESO 1 specific CD8$^+$ TILs were CD103$^+$ and CD39$^+$ (Supplementary Fig. S10A). Altogether, these data demonstrated that acquisition of the QP phenotype results from T cell stimulation in the tumor microenvironment and inferred that the QP population is solely composed of tumor specific T cells. This is consistent with the high expression of *MKI67*, encoding Ki 67, in QP clusters (**Fig. 3B**).

Significantly fewer CD28$^+$ cells among NY ESO 1 specific T cells from TILs was seen versus PBMCs (Supplementary Fig. S10B). Antigen specific T cells were CD28$^+$PD 1^{int} in PBMCs and CD28$^{+/}$ $^{-}$PD 1^{hi} at the tumor site. To examine the functional consequences of these opposite phenotypes, we stimulated circulating and tumor infiltrating CD8$^+$ T cells from NY ESO 1 seropositive patients with NY ESO 1 peptides in the absence or presence of blocking PD 1 mAb. Whereas PD 1 blockade led to enhanced growth of antigen specific T cells from PBMCs, no effect was observed on the proliferation of antigen specific T cells from TILs (**Fig. 5C**). PD 1 inhibition was not, however, ineffective at the tumor site, as it led to increased production of effector cytokines by antigen specific T cells (**Fig. 5D** and **E**).

IC-positive CD8$^+$ T cells predict clinical response to PD-1/PD-L1 blockade

Using quantitative multiplex IHC (30, 31), we assessed QP cells in pretreatment tumor samples from a cohort of 30 patients with metastatic or recurrent head and neck squamous cell carcinoma treated with ICB targeting the PD 1/PD L1 axis. The proportion of CD8$^+$ or QP TILs was then correlated to response to therapy and OS. Because TIM 3 was the final checkpoint acquired at the tumor site, we used it as a surrogate marker of the QP population. Examples of staining obtained in samples exhibiting a high or low TIM 3$^+$CD8$^+$ T cell infiltrate are shown in **Fig. 6A** (top and bottom, respectively). Quantification of QP (0.03% 15.98% of all nuclei, median 1.9) and total CD8$^+$ (0.15% 23.49% of all nuclei, median 5.57) TILs showed that their proportion was variable among patients. A correlation was observed between the CD8$^+$ infiltrate and response to therapy, although it did not reach statistical significance (**Fig. 6B**). Infiltration by QP cells significantly correlated with response to therapy and OS (**Fig. 6B** and **C**), whereas the total CD8$^+$ infiltrate did not significantly correlate with OS (**Fig. 6C**). The median survival of patients in the high and low CD8$^+$ T cell groups was 12.7 and 8.8 months, respectively. Median survival of patients with low QP infiltrate was 5.8 months, whereas that of patients with high QP infiltrate was not reached. These results corroborate the major contribution of QP cells to antitumor immunity.

Discussion

Our results put forward T cell exhaustion as an indicator of spontaneous adaptive immune response to tumors and, as such, as a biomarker of response to ICB. We showed that exhaustion was acquired at the tumor site through the sequential expression of ICs solely in tumor antigen specific T cells but not in bystander T cells. Specific cells additionally acquire Trm markers and CXCR6, allowing for their *in situ* residency. We also showed that exhausted Trm like cells were endowed with high cytotoxic and functional potential but have lost, for a large part, CD28 and TCF 1 expression. PD 1 blockade could revert functional exhaustion of tumor antigen specific CD8$^+$ TILs *in vitro*, while it enhanced proliferation of their circulating

tial, and sensitivity to PD 1 blockade supported their contribution to responsiveness to ICB *in vivo*, which was inferred by the correlation between the proportion of exhausted CD8$^+$ TILs and response to therapy and survival following ICB.

On the basis of murine models of chronic infection, exhausted T cells are proposed as a lineage of CD8$^+$ T cells distinct from memory T cells (4, 5). Our results showed that circulating tumor antigen specific CD8$^+$ T cells were memory CD28$^+$ cells. These cells, like nonexhausted memory circulating PD 1$^+$CD8$^+$ T cells from healthy individuals (40), expressed lower PD 1 compared with their tumor infiltrating counterparts. Accordingly, circulating tumor specific T cells, which did not express TIM 3 or CTLA 4, could substantially expand *in vitro* upon antigen stimulation, which was enhanced in the presence of anti PD 1. Murine models of exhaustion in cancer, largely relying on implantable syngeneic tumor cell lines, have quicker kinetics than human cancers. In one such model, transcription factors PRDM1 and c MAF are proposed to coordinate a coinhibitory gene module leading to the concomitant coexpression of several ICs (41). In agreement with these data, we showed that PRDM1 was more expressed in exhausted Trm like cells. However, our results argue in favor of a progressive acquisition of exhaustion with sequential gain of ICs accompanied by that of Trm markers. This is in agreement with the model that established degrees of exhaustion severity (21), where the transcription factor TOX is associated to exhaustion. Our data showed expression of TOX in QP cells and sequential gain of TOX expression at the tumor site. A study has shown, in a murine model of chimeric antigen receptor T cell transfer, that transferred T cells acquire an exhausted state at the tumor site through TOX and TOX2 dependent mechanisms (42).

Seminal work shows that CD8$^+$ TILs express Trm markers and that CD103 is involved both in T cell retention at the tumor site and in tumor recognition (10, 11). Another study shows that the ectonucleotidase CD39 is expressed in a subpopulation of CD103$^+$CD8$^+$ T cells enriched for tumor specificity (20). In agreement with these studies, we showed that Trm markers and CD39 expression is gained along the sequential acquisition of ICs and that they had high expression in antigen specific T cells. We also showed that exhausted cells exhibited lower S1PR1 expression, consistent with their *in situ* retention, and expressed the chemokine receptor CXCR6. CXCR6 is expressed in liver Trm cells (43), and its ligand, CXCL16, which can be produced in soluble and membrane bound forms (44), is expressed by tumor cells of different histologic types and is associated with increased tumor T cell infiltration (45). We propose that CXCR6 expression in exhausted Trm like cells facilitates their migration toward and their interaction with tumor cells.

We showed that TGFβ, involved in the induction of CD103 (9) as well as in high PD 1 expression (34), could also be implicated in CD28 loss. To our knowledge, this is not a function that has been attributed to TGFβ, although it is consistent with its immune suppressive role. Expression of SOX 4 and CXCL13 in the QP population further supported the involvement of TGFβ in its *in situ* development. Indeed, TGFβ induces SOX 4 (36, 37), which mediates CXCL13 production by CD4$^+$ T cells (37). CXCL13 has been involved in tertiary lymphoid structure (TLS) induction in inflammatory diseases (37), and its expression by tumor infiltrating CD8$^+$ T cells associates with high B cell recruitment and TLSs (46, 47).

PD L1 expression in peripheral tissues and the ability of PD 1 recruited SHP2 to dephosphorylate proteins involved in proximal TCR signaling implies a central role of PD 1 in blocking functions of effector T cells (13, 14). Studies show that PD 1 signaling inhibits CD28 more efficiently compared with TCR proximal signaling molecules (15), and,
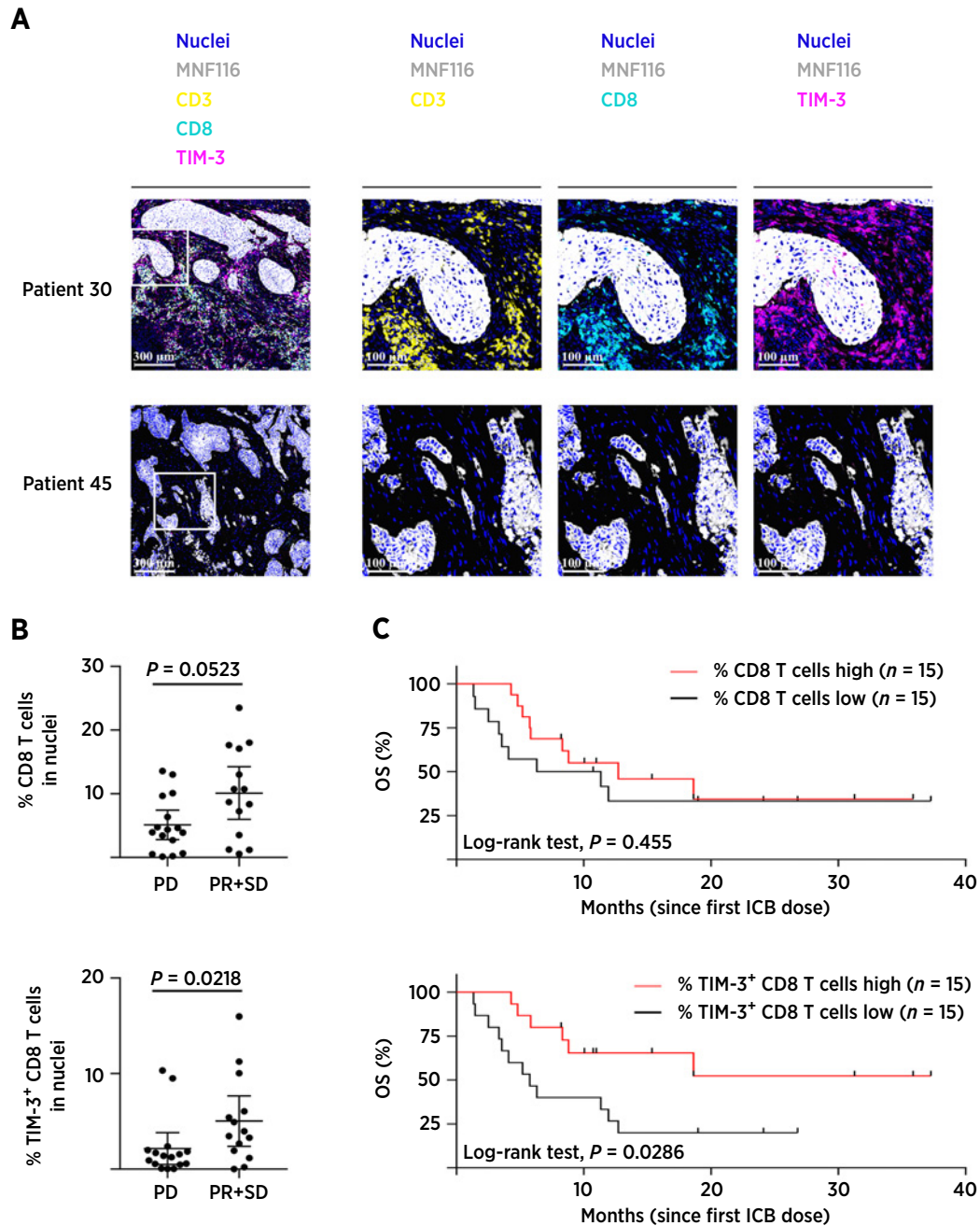
Figure 6.
IC positive Trm like exhausted CD8 T cells predict response to PD 1/PD L1 blockade and survival in HNC. Proportion of $CD8^+$ T cells and TIM 3^+CD8^+ T cells were determined using quantitative multiplex IHC in pretreatment tumor samples from 30 patients with HNC receiving anti PD 1/PD L1 and were correlated to clinical outcome. **A,** Representative images showing CD3 (yellow), CD8 (cyan), TIM 3 (magenta), and MNF116 (gray), as well as nuclei (blue) in two representative tumors with high (patient 30) and low (patient 45) QP infiltrate (left). Zoomed images at $3\times$ magnification (from boxed area in left image) are shown for the indicated markers (right). **B,** Frequency of $CD8^+$ T cells (top) and TIM 3^+ CD8 T cells (bottom) among all nuclei in patients with PD ($n = 16$) and patients with PR ($n = 6$) or SD ($n = 8$). **C,** Kaplan Meier curves of OS by high versus low frequency of total $CD8^+$ T cells (top, cutoff at median = 5.57%) or TIM 3^+ $CD8^+$ T cells (bottom, cutoff at median = 1.9%) among all nucleated cells. P values were determined with the Mann Whitney test (**B**); comparison of survival curves was determined with the log rank test (**C**).

accordingly, early proliferation of circulating PD $1^+CD28^+CD8^+$ T cells could be associated to response to ICB in patients with non small cell lung cancer (16, 17). We showed significant CD28 loss, specifically in exhausted tumor specific $CD8^+$ TILs. However, circulating antigen specific T cells were mostly $CD28^+$. Our functional analyses showed that *in vitro* PD 1 inhibition differentially modulated proliferation and effector functions in circulating and tumor infiltrating antigen specific T cells. These results are in agreement with previous

studies (15 17) and could imply that low PD 1 expression in circu lating antigen specific T cells will preferentially affect CD28 signaling, whereas overexpression of PD 1 in exhausted Trm like cells allows for inhibition of TCR signaling in addition to CD28. It is noteworthy that, in a reconstituted membrane *in vitro* setting, PD 1 mediated dephos phorylation of CD28 occurs at low PD 1 densities, whereas TCR signaling molecule dephosphorylation requires a higher density of PD 1 molecules (15), which could correspond to PD 1 densities found in PD 1^{hi} exhausted T cells.

Finally, in agreement with their tumor specificity and high cytotoxic and effector potential, exhausted Trm like T cells were predictive of response to ICB and survival in a cohort of patients with HNC. These results may contradict studies suggesting that TCF 1^+CD8$^+$ TILs, termed progenitor exhausted cells, are potential players in PD 1/PD L1 blockade *in vivo* efficacy (48 51). However, these studies largely rely on murine models whereby the degree of exhaustion attained in few weeks is not necessarily comparable with that found in patients. One study shows that TCF 1 expression in tumor antigen specific T cells in patients is detected in only a low proportion ($\sim$1%) of circulating antigen specific cells (51). Another study shows that the proportion of TCF 1^+ cells does not correlate with response to therapy but does correlate with survival in responder patients only (48). Another report found that the ratio between TCF 1^+ and TCF 1^- cells, rather than the proportion of positive cells, correlates to clinical responses (49). In our study, *TCF7* mRNA and TCF 1 protein were only detected in non QP cells at the tumor site. Our results showed significant correlation between TIM 3^+CD8$^+$ T cells, which did not express TCF 1, and both response to therapy and OS following ICB. These results do not exclude a potentially important role of TCF 1^+ tumor specific CD8$^+$ T cells in mediating response to therapy. We believe that the presence of TIM 3^+CD8$^+$ T cells is a direct indicator, that is, biomarker, of a spontaneous adaptive response to the tumor that can be mobilized by ICB. Altogether, our results imply that the combination of proliferation/reinvigoration of circu lating memory T cells, that will replenish the tumor site, combined to reversion of exhaustion, even temporary (6), at the tumor site con tribute to PD 1/PD L1 mediated tumor control.

Disclosure of Potential Conflicts of Interest

Authors' Contributions

Conception and design: C.-C. Balança, C.-M. Scarlata, M. Michelas, C. Devaud, V. Sarradin, J.-P. Delord, M. Ayyoub
Development of methodology: V. Sarradin, C. Martinez Gomez, M. Tosolini, F. Pont
Acquisition of data (provided animals, acquired and managed patients, provided facilities, etc.): C.-C. Balança, C.-M. Scarlata, M. Michelas, C. Devaud, V. Sarradin, C. Franchet, C. Martinez Gomez, C. Gomez-Roca, D. Heaugwane, F. Lauzéral-Vizcaino, L. Mir-Mesnier, V. Féliu, C. Valle, G. Ferron, L. Gladieff, S. Motton, Y. Tanguy Le Gac, A. Dupret-Bories, J. Sarini, B. Vairel, C. Illac, A. Siegfried-Vergnon, E. Mery, S. Vergez, J.-P. Delord, P. Rochaix
Analysis and interpretation of data (e.g., statistical analysis, biostatistics, computational analysis): C.-C. Balança, C.-M. Scarlata, M. Michelas, C. Devaud, V. Sarradin, C. Franchet, M. Tosolini, D. Heaugwane, F. Lauzéral-Vizcaino, L. Mir-Mesnier, V. Féliu, F. Pont, J.-J. Fournié, M. Ayyoub
Writing, review, and/or revision of the manuscript: C.-C. Balança, C.-M. Scarlata, M. Michelas, V. Sarradin, C. Franchet, C. Martinez Gomez, G. Ferron, L. Gladieff, J.-P. Delord, A. Martinez, M. Ayyoub
Administrative, technical, or material support (i.e., reporting or organizing data, constructing databases): C. Martinez Gomez
Study supervision: A. Martinez, M. Ayyoub

Acknowledgments

References

1. Fridman WH, Pagès F, Sautès-Fridman C, Galon J. The immune contexture in human tumours: impact on clinical outcome. Nat Rev Cancer 2012;12: 298–306.
2. Baumeister SH, Freeman GJ, Dranoff G, Sharpe AH. Coinhibitory pathways in immunotherapy for cancer. Annu Rev Immunol 2016;34:539–73.
3. Anderson AC, Joller N, Kuchroo VK. Lag-3, Tim-3, and TIGIT: co-inhibitory receptors with specialized functions in immune regulation. Immunity 2016;44: 989–1004.
4. McLane LM, Abdel-Hakeem MS, Wherry EJ. CD8 T cell exhaustion during chronic viral infection and cancer. Annu Rev Immunol 2019;37: 457–95.
5. Doering TA, Crawford A, Angelosanto JM, Paley MA, Ziegler CG, Wherry EJ. Network analysis reveals centrally connected genes and pathways involved in CD8+ T cell exhaustion versus memory. Immunity 2012;37: 1130–44.
6. Pauken KE, Sammons MA, Odorizzi PM, Manne S, Godec J, Khan O, et al. Epigenetic stability of exhausted T cells limits durability of reinvigoration by PD-1 blockade. Science 2016;354:1160–5.
7. Skon CN, Lee J-Y, Anderson KG, Masopust D, Hogquist KA, Jameson SC. Transcriptional downregulation of S1pr1 is required for the establishment of resident memory CD8+ T cells. Nat Immunol 2013;14:1285–93.
8. Cheuk S, Schlums H, Gallais Sérézal I, Martini E, Chiang SC, Marquardt N, et al. CD49a expression defines tissue-resident CD8+ T cells poised for cytotoxic function in human skin. Immunity 2017;46:287–300.
9. Mackay LK, Rahimpour A, Ma JZ, Collins N, Stock AT, Hafon M-L, et al. The developmental pathway for CD103(+)CD8+ tissue-resident memory T cells of skin. Nat Immunol 2013;14:1294–301.
10. Djenidi F, Adam J, Goubar A, Durgeau A, Meurice G, de Montpréville V, et al. CD8+CD103+ tumor-infiltrating lymphocytes are tumor-specific tissue-resident memory T cells and a prognostic factor for survival in lung cancer patients. J Immunol 2015;194:3475–86.
11. Franciszkiewicz K, Le Floc'h A, Jalil A, Vigant F, Robert T, Vergnon I, et al. Intratumoral induction of CD103 triggers tumor-specific CTL function and CCR5-dependent T-cell retention. Cancer Res 2009;69:6249–55.
12. Wei SC, Duffy CR, Allison JP. Fundamental mechanisms of immune checkpoint blockade therapy. Cancer Discov 2018;8:1069–86.

13. Freeman GJ, Long AJ, Iwai Y, Bourque K, Chernova T, Nishimura H, et al. Engagement of the PD-1 immunoinhibitory receptor by a novel B7 family member leads to negative regulation of lymphocyte activation. J Exp Med 2000; 192:1027–34.

14. Sheppard KA, Fitz LJ, Lee JM, Benander C, George JA, Wooters J, et al. PD-1 inhibits T-cell receptor induced phosphorylation of the ZAP70/CD3zeta signalosome and downstream signaling to PKCtheta. FEBS Lett 2004;574: 37–41.

15. Hui E, Cheung J, Zhu J, Su X, Taylor MJ, Wallweber HA, et al. T cell costimulatory receptor CD28 is a primary target for PD-1-mediated inhibition. Science 2017;355:1428–33.

16. Kamphorst AO, Wieland A, Nasti T, Yang S, Zhang R, Barber DL, et al. Rescue of exhausted CD8 T cells by PD-1-targeted therapies is CD28-dependent. Science 2017;355:1423–7.

17. Kamphorst AO, Pillai RN, Yang S, Nasti TH, Akondy RS, Wieland A, et al. Proliferation of PD-1+ CD8 T cells in peripheral blood after PD-1–targeted therapy in lung cancer patients. Proc Natl Acad Sci U S A 2017;114:4993–8.

18. Keir ME, Liang SC, Guleria I, Latchman YE, Qipo A, Albacker LA, et al. Tissue expression of PD-L1 mediates peripheral T cell tolerance. J Exp Med 2006;203: 883–95.

19. Ready N, Hellmann MD, Awad MM, Otterson GA, Gutierrez M, Gainor JF, et al. First-line nivolumab plus ipilimumab in advanced non-small-cell lung cancer (CheckMate 568): outcomes by programmed death ligand 1 and tumor mutational burden as biomarkers. J Clin Oncol 2019;37:992–1000.

20. Duhen T, Duhen R, Montler R, Moses J, Moudgil T, de Miranda NF, et al. Co-expression of CD39 and CD103 identifies tumor-reactive CD8 T cells in human solid tumors. Nat Commun 2018;9:2724.

21. Bengsch B, Ohtani T, Khan O, Setty M, Manne S, O'Brien S, et al. Epigenomic-guided mass cytometry profiling reveals disease-specific features of exhausted CD8 T cells. Immunity 2018;48:1029–45.

22. Stoeckius M, Hafemeister C, Stephenson W, Houck-Loomis B, Chattopadhyay PK, Swerdlow H, et al. Simultaneous epitope and transcriptome measurement in single cells. Nat Methods 2017;14:865–8.

23. Stuart T, Butler A, Hoffman P, Hafemeister C, Papalexi E, Mauck WM, et al. Comprehensive integration of single-cell data. Cell 2019;177:1888–902.

24. Herman JS, Sagar null, Grün D. FateID infers cell fate bias in multipotent progenitors from single-cell RNA-seq data. Nat Methods 2018;15:379–86.

25. Ashburner M, Ball CA, Blake JA, Botstein D, Butler H, Cherry JM, et al. Gene ontology: tool for the unification of biology. The gene ontology consortium. Nat Genet 2000;25:25–9.

26. Mi H, Huang X, Muruganujan A, Tang H, Mills C, Kang D, et al. PANTHER version 11: expanded annotation data from gene ontology and reactome pathways, and data analysis tool enhancements. Nucleic Acids Res 2017;45: D183–9.

27. The Gene Ontology Consortium. The Gene Ontology resource: 20 years and still GOing strong. Nucleic Acids Res 2019;47:D330–8.

28. Edgar R, Domrachev M, Lash AE. Gene Expression Omnibus: NCBI gene expression and hybridization array data repository. Nucleic Acids Res 2002; 30:207–10.

29. Redjimi N, Duperrier-Amouriaux K, Raimbaud I, Luescher I, Dojcinovic D, Classe JM, et al. NY-ESO-1-specific circulating CD4+ T cells in ovarian cancer patients are prevalently T(H)1 type cells undetectable in the CD25+ FOXP3+ Treg compartment. PLoS One 2011;6:e22845.

30. Glass G, Papin JA, Mandell JW. SIMPLE: a sequential immunoperoxidase labeling and erasing method. J Histochem Cytochem 2009;57:899–905.

31. Blom S, Paavolainen L, Bychkov D, Turkki R, Mäki-Teeri P, Hemmes A, et al. Systems pathology by multiplexed immunohistochemistry and whole-slide digital image analysis. Sci Rep 2017;7:15580.

32. Romero P, Zippelius A, Kurth I, Pittet MJ, Touvrey C, Iancu EM, et al. Four functionally distinct populations of human effector-memory CD8+ T lymphocytes. J Immunol 2007;178:4112–9.

33. Kotecha N, Krutzik PO, Irish JM. Web-based analysis and publication of flow cytometry experiments. Curr Protoc Cytom 2010;Chapter 10:Unit10.17.

34. Park BV, Freeman ZT, Ghasemzadeh A, Chattergoon MA, Rutebemberwa A, Steigner J, et al. TGFβ1-mediated SMAD3 enhances PD-1 expression on antigen-specific T cells in cancer. Cancer Discov 2016;6:1366–81.

35. Hu G, Chen J. A genome-wide regulatory network identifies key transcription factors for memory CD8$^+$ T-cell development. Nat Commun 2013;4:2830.

36. Kuwahara M, Yamashita M, Shinoda K, Tofukuji S, Onodera A, Shinnakasu R, et al. The transcription factor Sox4 is a downstream target of signaling by the cytokine TGF-β and suppresses TH2 differentiation. Nat Immunol 2012;13: 778–86.

37. Yoshitomi H, Kobayashi S, Miyagawa-Hayashino A, Okahata A, Doi K, Nishitani K, et al. Human Sox4 facilitates the development of CXCL13-producing helper T cells in inflammatory environments. Nat Commun 2018; 9:3762.

38. Wherry EJ, Blattman JN, Murali-Krishna K, Most R van der Ahmed R. Viral persistence alters CD8 T-cell immunodominance and tissue distribution and results in distinct stages of functional impairment. J Virol 2003;77:4911–27.

39. Bioley G, Guillaume P, Luescher I, Yeh A, Dupont B, Bhardwaj N, et al. HLA class I - associated immunodominance affects CTL responsiveness to an ESO recombinant protein tumor antigen vaccine. Clin Cancer Res 2009;15:299–306.

40. Duraiswamy J, Ibegbu CC, Masopust D, Miller JD, Araki K, Doho GH, et al. Phenotype, function, and gene expression profiles of programmed death-1(hi) CD8 T cells in healthy human adults. J Immunol 2011;186:4200–12.

41. Chihara N, Madi A, Kondo T, Zhang H, Acharya N, Singer M, et al. Induction and transcriptional regulation of the co-inhibitory gene module in T cells. Nature 2018;558:454–9.

42. Seo H, Chen J, González-Avalos E, Samaniego-Castruita D, Das A, Wang YH, et al. TOX and TOX2 transcription factors cooperate with NR4A transcription factors to impose CD8+ T cell exhaustion. Proc Natl Acad Sci U S A 2019;116: 12410–5.

43. Pallett LJ, Davies J, Colbeck EJ, Robertson F, Hansi N, Easom NJW, et al. IL-2^{high} tissue-resident T cells in the human liver: sentinels for hepatotropic infection. J Exp Med 2017;214:1567–80.

44. Matloubian M, David A, Engel S, Ryan JE, Cyster JG. A transmembrane CXC chemokine is a ligand for HIV-coreceptor Bonzo. Nat Immunol 2000;1:298–304.

45. Hojo S, Koizumi K, Tsuneyama K, Arita Y, Cui Z, Shinohara K, et al. High-level expression of chemokine CXCL16 by tumor cells correlates with a good prognosis and increased tumor-infiltrating lymphocytes in colorectal cancer. Cancer Res 2007;67:4725–31.

46. Thommen DS, Koelzer VH, Herzig P, Roller A, Trefny M, Dimeloe S, et al. A transcriptionally and functionally distinct PD-1+ CD8+ T cell pool with predictive potential in non-small-cell lung cancer treated with PD-1 blockade. Nat Med 2018;24:994–1004.

47. Workel HH, Lubbers JM, Arnold R, Prins TM, van der Vlies P, de Lange K, et al. A transcriptionally distinct CXCL13+CD103+CD8+ T-cell population is associated with B-cell recruitment and neoantigen load in human cancer. Cancer Immunol Res 2019;7:784–96.

48. Miller BC, Sen DR, Al Abosy R, Bi K, Virkud YV, LaFleur MW, et al. Subsets of exhausted CD8+ T cells differentially mediate tumor control and respond to checkpoint blockade. Nat Immunol 2019;20:326–36.

49. Sade-Feldman M, Yizhak K, Bjorgaard SL, Ray JP, de Boer CG, Jenkins RW, et al. Defining T cell states associated with response to checkpoint immunotherapy in melanoma. Cell 2018;175:998–1013.

50. Kurtulus S, Madi A, Escobar G, Klapholz M, Nyman J, Christian E, et al. Checkpoint blockade immunotherapy induces dynamic changes in PD-1-CD8+ tumor-infiltrating T cells. Immunity 2019;50:181–94.

51. Siddiqui I, Schaeuble K, Chennupati V, Fuertes Marraco SA, Calderon-Copete S, Pais Ferreira D, et al. Intratumoral Tcf1+PD-1+CD8+ T cells with stem-like properties promote tumor control in response to vaccination and checkpoint blockade immunotherapy. Immunity 2019;50:195–211.